IEEE Open Journal of
Power Electronics

Received 21 October 2021; revised 26 November 2021; accepted 5 December 2021. Date of publication 13 December 2021; date of current version 3 January 2022. The review of this article was arranged by Associate Editor Zhixiang Zou.

Digital Object Identifier 10.1109/OJPEL.2021.3134958

Optimized Reactive Power Control of Module Power Imbalance of Cascaded Converter

MIN CHEN (Senior Member, IEEE), YUFEI JIE, CHU WANG, GONGHENG LI, LIN QIU (Member, IEEE), AND WENXIN ZHONG (Senior Member, IEEE)

College of Electrical Engineering Institute of Power Electronics, Zhejiang University, Hangzhou 310027, China

CORRESPONDING AUTHORS: WENXIN ZHONG; MIN CHEN (e-mail: wxzhong@zju.edu.cn; heaven@zju.edu.cn)

This work was supported by the National Key R&D Program of China under Grant 2018YFB1500701.

ABSTRACT In the medium voltage cascaded converter, the power imbalance problem among the converter modules will result in certain converter modules over-modulated. Reactive power control (RPC) scheme is an effective way to balance the cascaded converters. Many efforts, such as reactive power sharing control and apparent power sharing control have been used to solve the overmodulation issue. This paper investigates an optimization RPC scheme to solve the overmodulation problem by minimizing the total required reactive power. An improved minimum reactive power (IMRP) RPC scheme is presented, the feasible area for the active power imbalance is evaluated and compared with the reactive power sharing control scheme and the apparent power sharing control scheme. Finally, the control scheme is verified on a three-module scaled-down cascaded inverter.

INDEX TERMS Reactive power control, cascaded converter, active power imbalance, photovoltaic.

I. INTRODUCTION

Continuously declining the cost of photovoltaic generation has promoted the rapid growth of PV installations [1], [2]. Solar energy is expected to be one of the dominant energies in the future. To reduce the per-wat cost of PV, the scale of centralized PV inverters is continuously increasing. Nowadays, the DC bus voltage is increased up to 1.5kV, and the power rating of the centralized inverter is increased up to MW. To further increase the inverter power, the MV inverter could be directly connected to the MV utility line. In this way, the bulky 50Hz transformer is needless, which not only saves space but also reduces the standby loss of the transformer.

The PV medium-voltage cascaded converters, which eliminate the bulky low-frequency transformer in conventional centralized PV plants, are potential candidates for next-generation utility-scale PV plants [3]–[8]. In the construction of high-efficiency cascaded photovoltaic systems, two conventional structures are the three-stage structure and the two-stage structure, which are depicted in Fig. 1 [9], [10]. In [10], the three-stage structure is used, the active power imbalance problem can be solved by the parallel connection of the first-stage power converter. Compared with the three-stage structure, the two-stage structure of Fig. 1(b) is more advantageous on efficiency and cost due to the reduction of power stages.

An important issue in the control system design of two-stage converters is active power imbalance. The output power of the PV panels varies with the change of irradiance, temperature, etc. In three-stage converters, the active power imbalance problem is solved by constructing a DC bus to distribute power through power modules. For two-stage converters, the DC bus is unavailable due to the absence of the front-end DC/DC converters. Thus, the active power imbalance is a critical problem for the PV medium-voltage two-stage cascaded converters.

Many sophisticated methods have been proposed to solve the active power imbalance problem. The simplest way is controlling the module voltage which is proportional to its active power[11]. The module with the largest active power will over-modulate easily under the power imbalance condition, as shown in Fig. 2(b). In [12], the voltage balance circuit is inserted between the power module to balance the active power. Some researchers found that the voltage balance circuit will increase the system cost and lower reliability and efficiency. And in [8], the three-port LLC converter is adopted as the isolated stage. A DC bus is built up using the third port

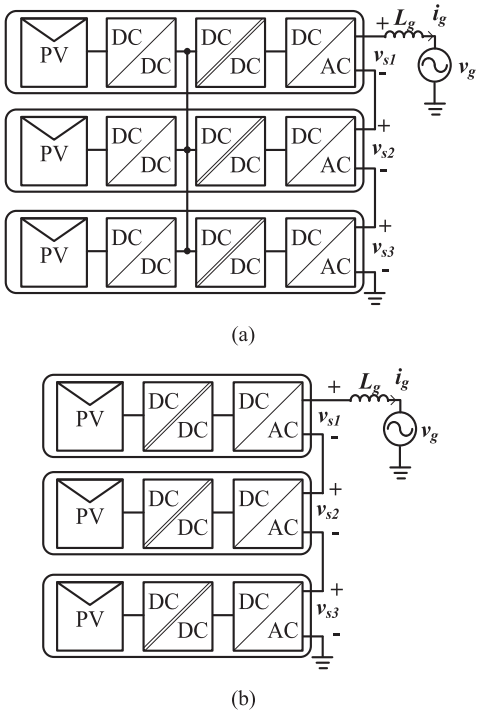

FIGURE 1. The structures of multi-stage converters in the PV system. (a) three-stage structure. (b) two-stage structure.

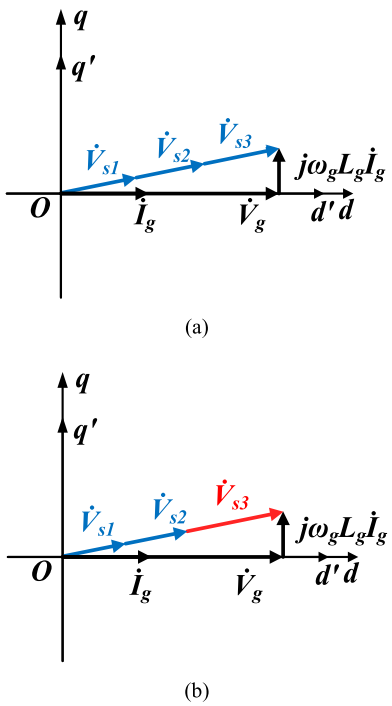

FIGURE 2. The phasor diagram under condition $P_g > 0$ and $Q_g = 0$. (a) Module phasor diagram under balance condition. (b) Module phasor diagram under imbalance condition.

to maintain power balance across modules. Some researchers found that this method needs some additional circuit elements.

Reactive power control (RPC) is an effective way to solve the overmodulation issue, which has an advantage in cost. Literature [13] proposed a control approach that autonomously compensates reactive power contents of inverters caused by the active and reactive power changes by shifting their phase angle with local AC current measurement. In [14], a reactive power control strategy is proposed for improving the converter's adaptability to the power imbalance. In this RPC scheme, the reactive power is evenly distributed to each power module, which is called as reactive power sharing (RPS) scheme. This control strategy is easy to be used, and some researchers found that the maximum power imbalance control adaptability is limited by the same reactive power control for each module. In [15], another RPC scheme is proposed where the apparent power of each power module is equal, which is called as apparent power sharing (APS) scheme. This control scheme efficiently improves the adaptability to the power imbalance, and the required reactive power is higher during some imbalance conditions, which will increase the power losses. In [16], the reactive power for each power module is distributed inversely to its corresponding active power. This control scheme improves adaptability and it also required more reactive power.

Apart from the RPC scheme, other methods, such as common mode injection[17], [18], third harmonic injection[19], [20], space vector modulation[21], or square-wave modulation[22], are also proposed to improve the adaptability of the cascaded photovoltaic converters. Due to the limitation of the modulation ratio, the RPC scheme is a more efficient method for the module active power imbalance problem. The RPC scheme can be easily combined with these modulation schemes [15], [22], [23], which will further improve the adaptability of the cascaded photovoltaic converters.

Two key indexes of the RPC scheme are the tolerance range of active power imbalance and the minimum required reactive power. Less reactive power means lower power losses of the converter, i.e., higher efficiency of the converter.

This paper proposes an improved reactive power control scheme of enhancing adaptability to the power imbalance. It is based on the idea of minimum reactive power distributing and adding reactive power calculation control loops for each power module. The proposed scheme is designed to achieve a wider tolerance range and less reactive power.

This paper is organized as follows. Section I introduces the background of the active power imbalance control method for the cascade inverter. Section II analyzes the inverter operating feasible area under active power imbalance conditions for the traditional RPC scheme. Section III describes the improved RPC scheme with the minimum required reactive power. Section IV analyzes the inverter operating feasible area for the proposed control scheme. A scaled-down prototype is built up and the experimental results verify the proposed RPC scheme in Section V.

II. ANALYSIS OF THE CASCADED PV CONVERTER UNDER POWER IMBALANCE CONDITION

A. THE POWER IMBALANCE PROBLEM

For simplicity, a cascaded PV converter with 3 modules is considered in this paper, as shown in Fig. 1. Assuming the active power, reactive power, and apparent power of each module is P_i, Q_i, and S_i, respectively. The fundamental RMS value element of an output voltage for each module is V_{si}. The fundamental RMS value of the total output voltage is V_s. The fundamental RMS value of the grid voltage and current are V_g and I_g, respectively. P_g is the total output active power, Q_g is the total output reactive power.

The phasor diagram with $P_g > 0$ and $Q_g = 0$ is depicted in Fig. 2. To distinguish the active and reactive elements of the grid current I_g, the d axis is aligned with the grid voltage phasor and the q axis is lagged d axis by 90 degrees. Also, to distinguish the active and reactive components of the output voltage V_s, the d' axis is aligned with the grid current $\dot{I}_g$ and the q' axis is lagged d' axis by 90 degrees.

The relationship between the total output voltage $\dot{V}_s$, the grid voltage $\dot{V}_g$, and the grid current $\dot{I}_g$ is

$$\dot{V}_s = \dot{V}_g + jX_L\dot{I}_g \tag{1}$$

where $X_L = \omega_g L_g$. ω_g is the angular frequency of the grid voltage, L_g is the filter inductor.

When power modules don't output reactive power, the output voltage of each power module $\dot{V}_{si}$ is proportional to the corresponding module active power P_i, which is

$$\dot{V}_{si} = \frac{P_i}{P_g}\dot{V}_s \tag{2}$$

When the output power P_i is balanced, i.e., $P_1{=}P_2{=}P_3$, the output voltage magnitude of each power module will be the same, i.e., $V_{s1}{=}V_{s2}{=}V_{s3}$. The phasor diagram is depicted in Fig. 2(a). When the output power P_i is unbalanced, such as $P_1{<}P_2{<}P_3$, the output voltage V_{s3} will be the largest magnitude among the three power converter modules. In some cases, when the power imbalance is serious, module 3 will tend to be over-modulated, as shown in Fig. 2(b). The over-modulation might result in instability and higher current THD. Reactive power control [13]–[15] is a good solution to adapt to the power imbalance.

B. ANALYSIS OF THE CONVENTIONAL RPC SCHEMES

In this section, the aforementioned RPS and APS schemes will be analyzed. The feasible area of these two schemes and the required reactive power will be calculated.

The output voltage d' components of each module $V_{sid'}$ can be calculated as:

$$V_{sid'} = \frac{P_i}{P_g}V_{sd'} = \frac{P_i}{P_g}\frac{P_g}{\sqrt{P_g^2 + Q_g^2}}V_g = \frac{P_i}{\sqrt{\left(\sum_{i=1}^{N} P_i\right)^2 + \left(\sum_{i=1}^{N} Q_i\right)^2}}V_g \tag{3}$$

where $V_{sd'}$ is the d' components of total output voltage, N is the Module number.

By ignoring the impact of the filter inductor in (1), the output voltage q' components of each module $V_{siq'}$ can be calculated as

$$V_{siq'} = \frac{Q_i}{Q_g}V_{sq'} \approx \frac{Q_i}{Q_g}\frac{Q_g}{\sqrt{P_g^2 + Q_g^2}}V_g = \frac{Q_i}{\sqrt{\left(\sum_{i=1}^{N} P_i\right)^2 + \left(\sum_{i=1}^{N} Q_i\right)^2}}V_g \tag{4}$$

where $V_{sq'}$ is the q' components of total output voltage. With (3), (4), the output voltage of the inverter side is

$$V_{si} \approx \frac{S_i}{S_g}V_g = \frac{\sqrt{P_i^2 + Q_i^2}}{\sqrt{\left(\sum_{i=1}^{N} P_i\right)^2 + \left(\sum_{i=1}^{N} Q_i\right)^2}}V_g \tag{5}$$

For the RPS scheme, the reactive power of each module will be the same, that is [14]

$$Q_i = \frac{Q_g}{N} \tag{6}$$

N is the number of the power modules. The output voltage of each power module is limited by V_{max}, which is

$$V_{si} \le V_{max} \tag{7}$$

By limiting the voltage of the power module at V_{max}, the required minimum reactive power for the RPS scheme can be calculated from(5), (6), which is

$$Q_g = \sqrt{\frac{P_m^2 - (V_{max}/V_g)^2 P_g^2}{(V_{max}/V_g)^2 - 1/N^2}} \tag{8}$$

where P_m is the output active power of the power module which outputs the maximum active power.

Besides the limitation of the power module output voltage, the power module apparent power should not exceed the maximum allowable value S_{max}, which is

$$\begin{cases} P_1^2 + (Q_g/N)^2 \le S_{max}^2 \\ P_2^2 + (Q_g/N)^2 \le S_{max}^2 \\ P_3^2 + (Q_g/N)^2 \le S_{max}^2 \end{cases} \tag{9}$$

The boundaries of the feasible area for the RPS scheme in (9) are shown in Fig. 3(a). The red line is the output voltage limitation of module 1, the green line is the output voltage limitation of module 2, the blue line is the output voltage limitation of module 3. The feasible area of the RPS scheme is the intersection of the feasible area of three modules. The parameters used in the calculation are listed in Table 1. The active power of P_3 is 70 kW.

For the APS scheme, the module apparent powers are controlled to be the same. The reactive power of each module can be calculated by [15]:

$$Q_g = \sum_{i=1}^{N} \sqrt{S_{ref}^2 - P_i^2} \tag{10}$$

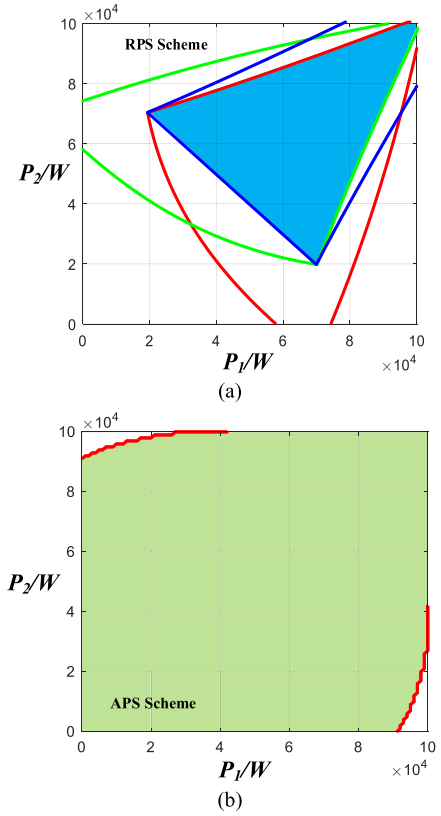

FIGURE 3. The feasible area of the RPS and APS scheme with $P_3 = 70$ kW. (a) RPS scheme. (b) APS scheme.

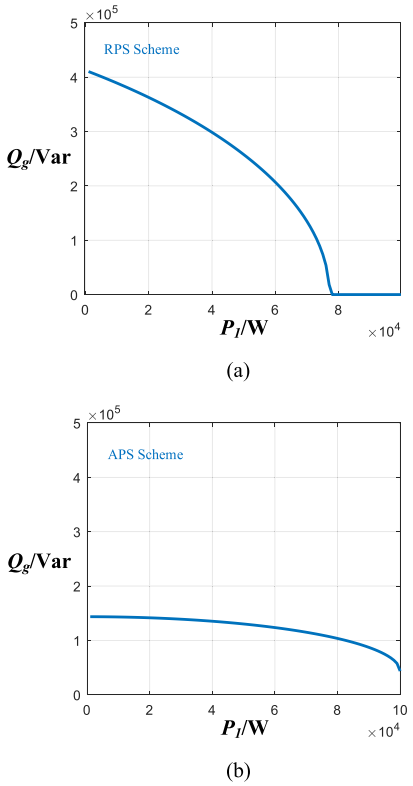

FIGURE 4. The required reactive power of the RPS, APS schemes with $P_2 = 90$ kW and $P_3 = 100$ kW. (a) RPS scheme. (b) APS scheme.

TABLE 1 System Parameters

Three-Module Photovoltaic System Parameters	
Parameters	Value
Grid Voltage V_g	1700V
Module DC bus Voltage V_{dci} (i=1, 2, 3)	1000V
Module Capacity S_{max}	100kVA
Grid Inductor L_g	700μH
Module Number N	3
Max modulation index m_{max}	0.9
Max Module Output Voltage (RMS) V_{max}	636V

where the apparent power of each module S_{ref} can be calculated by[15],

$$f(S_{ref}) = \frac{S_{ref}}{\sqrt{P_g^2 + \left(\sum_{i=1}^{N}\sqrt{S_{ref}^2 - P_i^2}\right)^2}} V_g$$
$$\begin{cases} S_{ref} = P_m, V_{si} = f(S_{ref}) < V_{max} \\ S_{ref} = solve[f(S_{ref}) = V_{max}], V_{si} = f(S_{ref}) = V_{max} \end{cases} \quad (11)$$

The boundaries of the feasible area for the APS scheme in (12) are shown in Fig. 3(b).

It can be seen from Fig. 3(b) that the feasible area of the APS scheme is different from the RPS scheme.

$$S_{ref} \le S_{max} \quad (12)$$

The minimum required reactive power of the RPS scheme and APS scheme in (8) and (10) are shown in Fig. 4.

III. THE PROPOSED REACTIVE POWER CONTROL SCHEME

Since the basic idea of the proposed scheme is minimizing the reactive power, the proposed scheme is called an improved minimum reactive power (IMRP) control scheme.

A. THE CONTROL SYSTEM OF THE IMRP SCHEME

In order to reduce the minimum required reactive power and extend the unbalanced active power feasible area, this paper proposed an optimization RPC scheme to solve the over-modulation problem by minimizing the total required reactive power and adding a module reactive power calculation control loop. The control system diagram proposed in this paper is depicted in Fig. 5.

The proposed control system contains 7 units. The DC voltage control module samples the input DC voltage of each power module V_{dci} and calculates the module active power P_i. The module active powers P_1 to P_N are then sorted in the active power sorting unit as:

$$P_{k1} \le P_{k2} \le \cdots \le P_{kN} \quad (13)$$

The sorted active powers P_{ki} are input to the reactive power calculation unit, where the total reactive power Q_g and the reactive power of each module Q_{ki} will be calculated. The Q_g and the P_g will then be sent to the current control unit. The reference current i_{dref} and i_{qref} will be calculated by P_g and Q_g. The output of the current control unit is the d'-q' components of the system output voltage, i.e., $v_{sd'}$ and $v_{sq'}$. The module

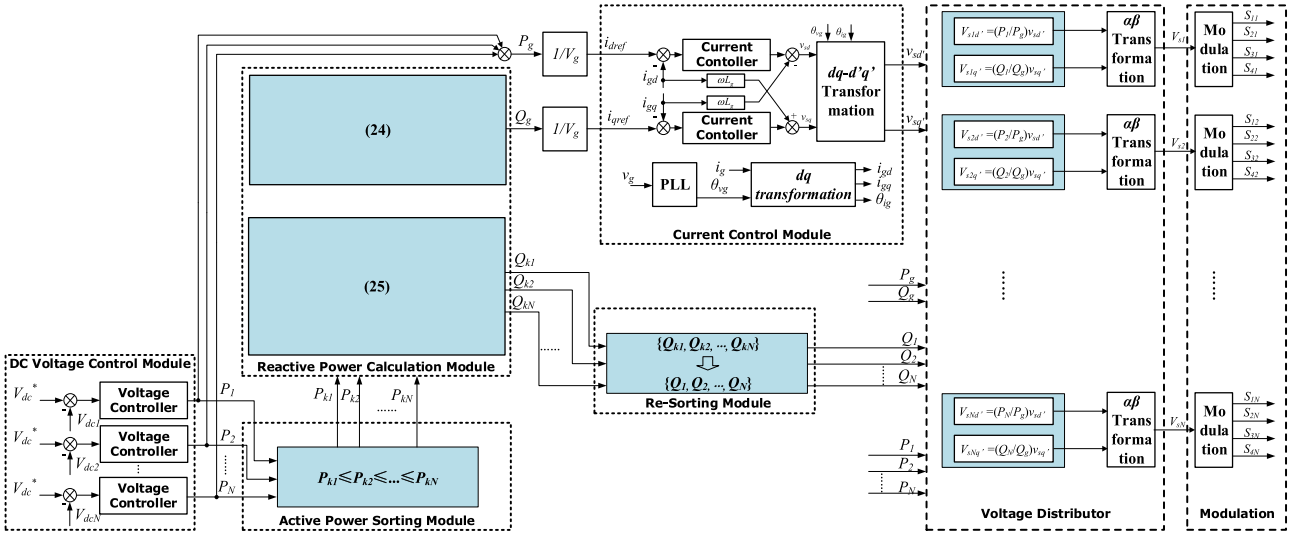

FIGURE 5. The IMRP control system diagram.

reactive power Q_{ki} is re-sorted to Q_i in the re-sorting unit. The P_i, Q_i, P_g, and Q_g are used to distribute the $v_{sd'}$ and $v_{sq'}$ to each of the power modules and the output voltage v_{si} of each power module are derived in the voltage distributor unit. Finally, the v_{si} are passed through the modulation unit and the switching signals are generated to control the power switches. The phase angle of the grid current θ_{ig} is,

$$\theta_{ig} = \theta_{vg} + \arctan\left(\frac{Q_g}{P_g}\right) \tag{14}$$

Where Q_g is the total reactive power, P_g is the total active power, the grid voltage phase θ_{vg} is obtained through a phase locked loop (PLL).

The key component of the proposed control system is the reactive power calculation module, in which the aggregate reactive power Q_g and module reactive power Q_i are determined. Q_i is the re-sort result of Q_{ki}.

B. THE REACTIVE POWER CALCULATION OF THE IMRP SCHEME

For simplicity, this section considers a cascaded PV converter with three modules to derive the equation of Q_g and Q_{ki}.

To avoid over-modulation, the module voltage V_i shouldn't exceed the maximum voltage V_{max}.

$$V_{si} = \sqrt{V_{sid'}^2 + V_{siq'}^2} \le V_{\max} \tag{15}$$

According to (3) (15):

$$V_{siq'} \le \sqrt{V_{\max}^2 - V_{sid'}^2} = \sqrt{V_{\max}^2 - \left(\frac{P_i}{\sqrt{P_g^2 + Q_g^2}}\right)^2} \tag{16}$$

To solve Q_g, take the equivalent transformation of (16):

$$Q_g^2 \ge \frac{V_g^2}{V_{\max}^2 - V_{siq'}^2} P_i^2 - P_g^2 \tag{17}$$

When the output power P_i is unbalanced, such as $P_1 < P_2 < P_3$, the output voltage V_{s3} will be the largest among the three power converter modules. In the actual operation of the three modules converter, V_{s3} is most likely to over-modulation. So, when Q_g is low, the $V_{s3q'}$ is set to zero. Based on the above analysis:

$$Q_g = \sqrt{\frac{V_g^2}{V_{\max}^2} P_i^2 - P_g^2} \tag{18}$$

The cascaded PV converter has four operating conditions: without over-modulation, slightly over-modulation, moderate over-modulation, and serious over-modulation.

The first operating condition is without over-modulation. When (18) has no real solution, the reactive power injected is needless. In this condition, the active power imbalance is absence. The calculation of Q_g and Q_{ki} are shown in (19). The without over-modulation vector diagram is shown in Fig. 6(a).

$$\begin{cases} Q_g = 0 \\ Q_{k1} = Q_{k2} = Q_{k3} = 0 \end{cases}, \left(\frac{V_g}{V_{\max}} P_3\right)^2 - P_g^2 \le 0 \tag{19}$$

The second operating condition is slightly over-modulation. In this condition, only the active power smallest module injects the reactive power. The calculation of Q_g and Q_{ki} are shown in (20). The slightly over-modulation vector diagram is shown in Fig. 6(b). The module phasor diagram of slightly

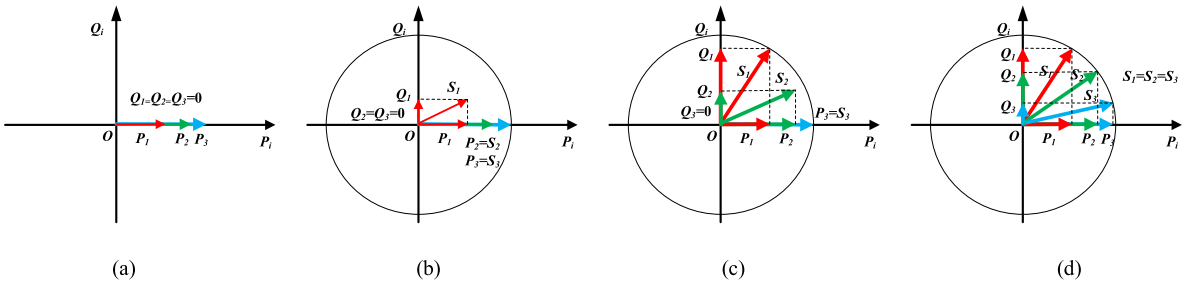

FIGURE 6. The vector diagram of the IMRP scheme. (a) Without over-modulation vector diagram. (b) Slightly over-modulation vector diagram. (c) Moderate over-modulation vector diagram. (d) Serious over-modulation vector diagram.

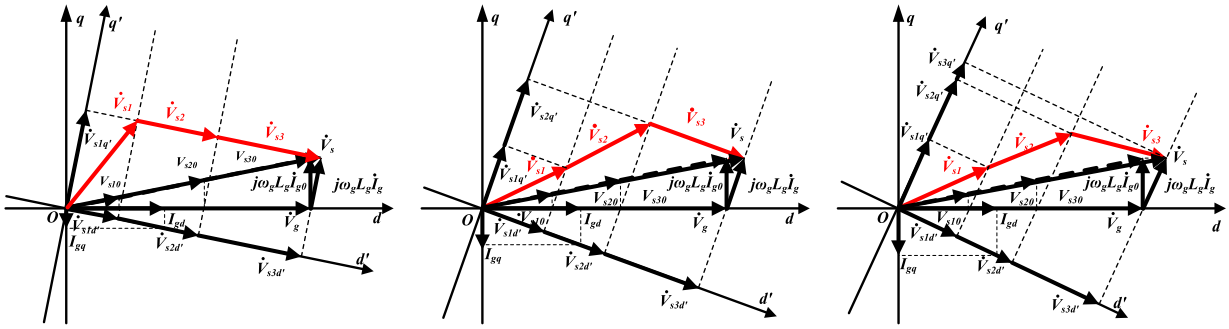

FIGURE 7. The module phasor diagram of the IMRP scheme. (a) The module phasor diagram of slightly over-modulation. (b) The module phasor diagram of moderate over-modulation. (c) The module phasor diagram of serious over-modulation.

over-modulation is shown in Fig. 7(a).

$$\begin{cases} Q_g = \sqrt{\left(\frac{V_g}{V_{\max}}P_3\right)^2 - P_g^2} \\ Q_{k1} = \sqrt{\left(\frac{V_g}{V_{\max}}P_3\right)^2 - P_g^2} \\ Q_{k2} = Q_{k3} = 0 \end{cases}, \quad 0 \le \sqrt{\left(\frac{V_g}{V_{\max}}P_3\right)^2 - P_g^2} \le \sqrt{P_3^2 - P_1^2} \tag{20}$$

The third operating condition is moderate over-modulation. In this condition, both module 1 and module 2 inject the reactive power. The calculation of Q_g and Q_{ki} are shown in (21). The moderate over-modulation vector diagram is shown in Fig. 6(c). The module phasor diagram of moderate over-modulation is shown in Fig. 7(b).

$$\begin{cases} Q_g = \sqrt{\left(\frac{V_g}{V_{\max}}P_3\right)^2 - P_g^2} \\ Q_{k1} = \sqrt{P_3^2 - P_1^2} \\ Q_{k2} = \sqrt{\left(\frac{V_g}{V_{\max}}P_3\right)^2 - P_g^2} - \sqrt{P_3^2 - P_1^2} \\ Q_{k3} = 0 \end{cases}, \quad \sqrt{P_3^2 - P_1^2} \le \sqrt{\left(\frac{V_g}{V_{\max}}P_3\right)^2 - P_g^2} \le \sum_{j=1}^{2}\sqrt{P_3^2 - P_j^2} \tag{21}$$

The last operating condition is serious over-modulation. In this condition, all three modules inject the reactive power. The calculation of Q_g and Q_{ki} are shown in (22). The serious over-modulation vector diagram is shown in Fig. 6(d). The module phasor diagram of serious over-modulation is shown in Fig. 7(c).

$$\begin{cases} Q_g = \sum_{j=1}^{3}\sqrt{S_{ref}^2 - P_j^2} \\ Q_{k1} = \sqrt{S_{ref}^2 - P_1^2} \\ Q_{k2} = \sqrt{S_{ref}^2 - P_2^2} \\ Q_{k3} = \sqrt{S_{ref}^2 - P_3^2} \end{cases}, \quad \sqrt{\left(\frac{V_g}{V_{\max}}P_3\right)^2 - P_g^2} > \sum_{j=1}^{2}\sqrt{P_3^2 - P_j^2} \tag{22}$$

Where the S_{ref} is calculated by solving the equation (23), which is a transcendental equation. This paper uses binary search to solve this equation. The precision of binary search is set as 5%.

$$\frac{S_{ref}}{\sqrt{\left(\sum_{i=1}^{N}P_{ki}\right)^2 + \left(\sum_{i=1}^{N}\sqrt{S_{ref}^2 - P_{ki}^2}\right)^2}}V_g = V_{max} \tag{23}$$

Extend the formulas of Q_g and Q_{ki} to the general case. The cascaded PV converter has N modules and the active power numerical relationship is random. The equations calculating

the Q_g and the Q_{ki} are:

$$Q_g = \begin{cases} 0, \\ \left(\frac{V_g}{V_{\max}}P_{kN}\right)^2 - P_g^2 \le 0 \\ \sqrt{\left(\frac{V_g}{V_{\max}}P_{kN}\right)^2 - P_g^2}, \\ 0 \le \left(\frac{V_g}{V_{\max}}P_{kN}\right)^2 - P_g^2 \le \left(\sum_{j=1}^{N-1}\sqrt{P_{kN}^2 - P_{kj}^2}\right)^2 \\ \sum_{j=1}^{N}\sqrt{S_{ref}^2 - P_{kj}^2}, \\ \left(\frac{V_g}{V_{\max}}P_{kN}\right)^2 - P_g^2 > \left(\sum_{j=1}^{N-1}\sqrt{P_{kN}^2 - P_{kj}^2}\right)^2 \end{cases} \tag{24}$$

$$Q_{ki} = \begin{cases} 0, \\ \sqrt{\left(\frac{V_g}{V_{\max}}P_{kN}\right)^2 - P_g} - \sum_{j=1}^{i-1}Q_{kj} < 0 \\ \sqrt{\left(\frac{V_g}{V_{\max}}P_{kN}\right)^2 - P_g^2} - \sum_{j=1}^{i-1}Q_{kj}, \\ 0 \le \sqrt{\left(\frac{V_g}{V_{\max}}P_{kN}\right)^2 - P_g^2} - \sum_{j=1}^{i-1}Q_{kj} < \sqrt{P_{kN}^2 - P_{ki}^2} \\ \sqrt{P_{kN}^2 - P_{ki}^2}, \\ \sqrt{P_{kN}^2 - P_{ki}^2} \le \sqrt{\left(\frac{V_g}{V_{\max}}P_{kN}\right)^2 - P_g^2} - \sum_{j=1}^{i-1}Q_{kj} \\ < \sum_{j=1}^{N-1}\sqrt{P_{kN}^2 - P_{kj}^2} - \sum_{j=1}^{i-1}Q_{kj} \\ \sqrt{S_{ref}^2 - P_{ki}^2}, \\ \left(\frac{V_g}{V_{\max}}P_{kN}\right)^2 - P_g^2 > \left(\sum_{j=1}^{N-1}\sqrt{P_{kN}^2 - P_{kj}^2}\right)^2 \end{cases} \tag{25}$$

The basic idea of the proposed scheme is to determine the minimum required reactive power Q_g and distribute the Q_g to each of the power modules in a reasonable way. Specifically, when the power imbalance is relatively slight, the required reactive power Q_g is relatively small, thus only part of the power modules are controlled to output reactive power. On the other hand, when the power imbalance is relatively serious, more power modules will be driven to support the increasing reactive power requirement.

The minimum required reactive power is listed in (24). The first line of (24) means that there is no need to output the reactive power. The second line of (24) means that the module which outputs maximum active power doesn't need to output the reactive power, the output voltage of the maximum active power module reaches the maximum value V_{max}. The third line of (24) means that all modules need to output the reactive power with the same apparent power.

The output reactive power for each module is listed in (25). The first line of (25) means that this module does not need to output the reactive power. The second line of (25) means that this module can output the remaining reactive power. The third line of (25) means that this module outputs the maximum reactive power. The fourth line of (25) means that all the module outputs the same apparent power. The flow chart of the reactive power calculation is shown in Fig. 8.

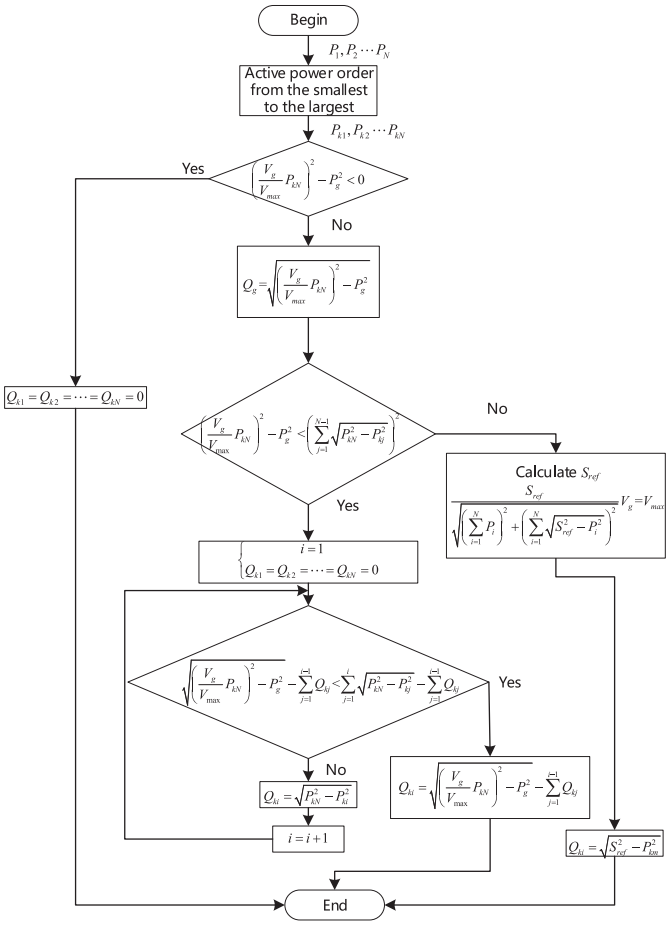

FIGURE 8. The flow chart of the reactive power calculation.

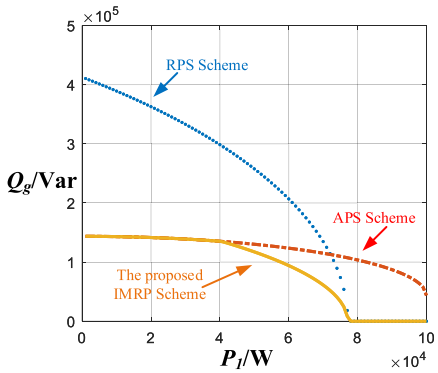

FIGURE 9. The required reactive power of three RPC schemes with P_2 = 90 kW and P_3 = 100 kW.

C. THE MINIMUM REQUIRED REACTIVE POWER AND THE FEASIBLE AREA OF THE IMRP SCHEME

The minimum required reactive power of the IMRP scheme is depicted in Fig. 9. It can be seen from Fig. 9 that the reactive power of the proposed IMRP scheme is not larger than both the APS and RPS scheme.

The feasible area of the proposed IMRP scheme is

$$S_{ref} \le S_{max} \tag{26}$$

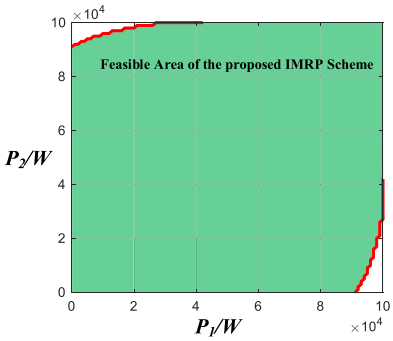

FIGURE 10. The feasible area of the IMRP scheme with P_3=70 kW.

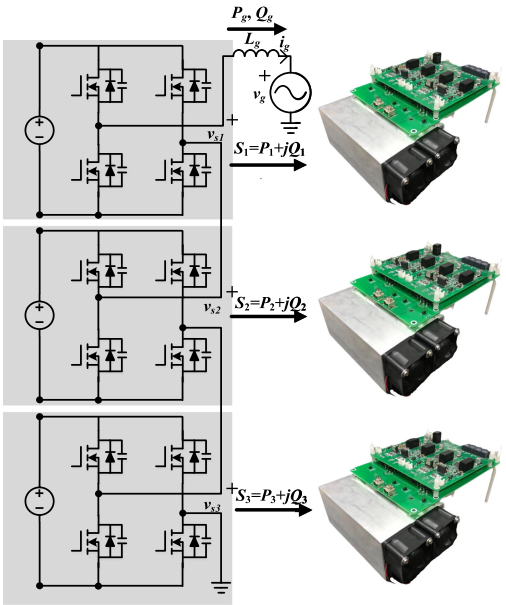

FIGURE 11. The experimental prototype circuit diagram.

Where the S_{ref} is calculated by (23). The feasible area result for $P_1 = 0{\sim}100$ kW, $P_2 = 0{\sim}100$ kW, and $P_3 = 70$ kW is depicted in Fig. 10 . It can be seen from Fig. 10 and Fig. 3, the feasible area of the proposed IMRP scheme is not smaller than both the APS and RPS scheme.

Compared with the RPS scheme in reference [14] and the APS scheme in reference [15], the advantage of the proposed IMRP scheme is that it minimizes the reactive power required by the system. The reactive power of the proposed IMRP scheme is not larger than both the APS and RPS scheme under all working conditions and the feasible area of the proposed IMRP scheme is not smaller than both the APS and RPS scheme.

IV. EXPERIMENTAL RESULTS

To verify the proposed scheme, a 3kVA three-module cascaded PV converter prototype is built up, the main circuit is shown in Fig. 11. The parameters of the prototype are listed in Table 2. Based on the experimental parameters, the feasible area of the IMRP scheme is depicted in Fig. 12. The feasible area of the RPS and APS scheme is depicted in Fig. 13.

Fig. 14 shows the required reactive power of three PRC schemes with $P_2 = 400$ W, $P_3 = 500$ W. It can be seen from Figs. 12–14 that the IMRP scheme has a larger feasible area

TABLE 2 Three-Module Scaled-Down Prototype Parameters

Parameters	Value
Grid Voltage V_g	220V
Module DC bus Voltage V_{dci} (i=1, 2, 3)	140V
Module Capacity S_{max}	1kVA
Grid Inductor L_g	700μH
Module Number N	3
Max modulation index m_{max}	0.85

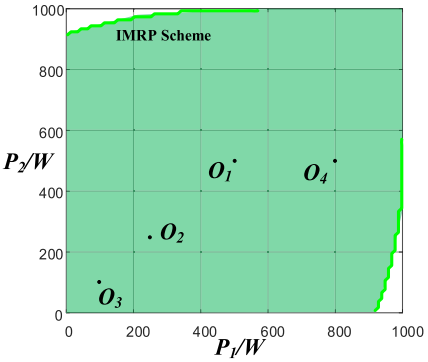

FIGURE 12. The feasible Area of the IMRP scheme with P3 = 500 W.

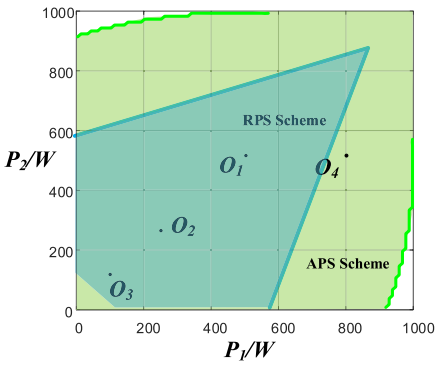

FIGURE 13. The feasible Area of the RPS and APS scheme with P_3=500W.

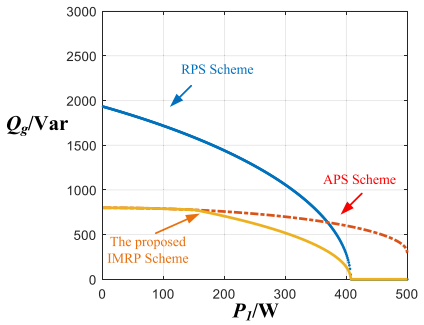

FIGURE 14. The required reactive power of three RPC schemes with P_2 = 400 W and P_3 = 500 W.

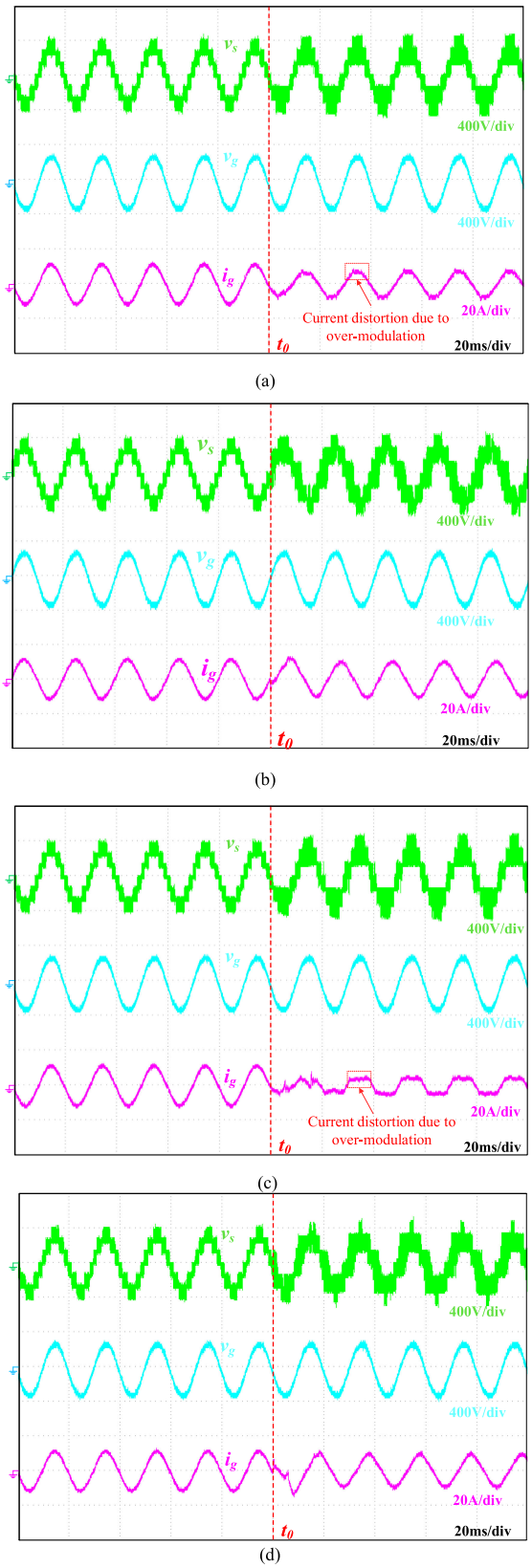

FIGURE 15. The transient waveforms under different imbalance conditions. (a) Switching from O1 to O2 without reactive power injection. (b) Switching from O1 to O2 with reactive power injection. (c) Switching from O1 to O3 without reactive power injection. (d) Switching from O1 to O3 with reactive power injection.

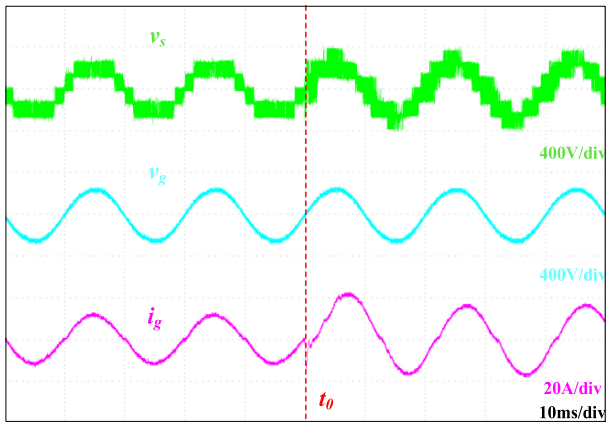

FIGURE 16. Switching from O_1 to O_4 with the IMRP scheme.

and smaller required reactive power than the RPS scheme. It can be seen from Figs. 12 and 13 that the IMRP scheme has the same feasible area as the APS scheme and it can be seen from Fig. 14 that the IMRP scheme has smaller required reactive power than the APS scheme. Three operation conditions, O_1 ($P_1 = P_2 = P_3 = 500$ W), O_2 ($P_1 = P_2 = 250$ W, $P_3 = 500$ W), O_3 ($P_1 = 100$ W, $P_2 = 100$ W, $P_3 = 500$ W) are chosen. The operation curves without reactive power injection (before t_0) are shown in Fig. 15(a) and (c). Before t_0, the system works at balance condition O_1. At time t_0, the system is switched to imbalance conditions. The system operation curves under O_2 and O_3 (after t_0) are shown in Fig. 15(a) and (c), respectively. It can be seen from the figures that the output current will be distorted under imbalance conditions with $Q_g = 0$. The distortion will become more serious with the imbalance getting worse. The operation curves using the proposed IMRP control scheme are shown in Fig. 15(b) and (d). It can be seen from these figures that the system works normally under imbalanced conditions. The transient performance of the proposed IMRP control scheme is also verified. As can be seen from these figures, the switching interval between different imbalance conditions is shorter than one single fundamental period. In order to verify that the IMRP scheme has a larger feasible area than the RPS and APS, O_4 ($P_1 = 800$ W, $P_2 = P_3 = 500$ W) is chosen. As shown in Figs. 12 and 13, only the IMRP scheme can work in this operation. The operation curves are shown in Fig. 16. It can be seen that the system works normally.

V. CONCLUSION

This paper discusses the RPC scheme for controlling the power imbalance of cascaded photovoltaic converter. Based on the detailed mathematical analysis, the proposed IMRP scheme reasonably distributes the reactive power to every power module. The feasible area and required reactive power of the IMRP scheme are also analyzed. The proposed IMRP scheme not only improves the adaptability of the cascaded photovoltaic converter but also reduces the required reactive power. The theoretical and experimental results show that the

proposed IMRP scheme can operate under imbalanced active power conditions.

REFERENCES

[1] S. Bacha, D. Picault, B. Burger, I. Etxeberria-Otadui, and J. Martins, "Photovoltaics in microgrids: An overview of grid integration and energy management aspects," *IEEE Ind. Electron. Mag.*, vol. 9, no. 1, pp. 33–46, Mar. 2015, doi: 10.1109/MIE.2014.2366499.

[2] S. Kouro, J. I. Leon, D. Vinnikov, and L. G. Franquelo, "Grid-connected photovoltaic systems: An overview of recent research and emerging PV converter technology," *IEEE Ind. Electron. Mag.*, vol. 9, no. 1, pp. 47–61, Mar. 2015, doi: 10.1109/MIE.2014.2376976.

[3] B. Zhao, Q. Song, J. Li, X. Xu, and W. Liu, "Comparative analysis of multilevel-high-frequency-link and multilevel-dc-link DC–DC transformers based on MMC and dual-active bridge for MVDC application," *IEEE Trans. Power Electron.*, vol. 33, no. 3, pp. 2035–2049, Mar. 2018, doi: 10.1109/TPEL.2017.2700378.

[4] M. R. Islam, A. M. Mahfuz-Ur-Rahman, M. M. Islam, Y. G. Guo, and J. G. Zhu, "Modular medium-voltage grid-connected converter with improved switching techniques for solar photovoltaic systems," *IEEE Trans. Ind. Electron.*, vol. 64, no. 11, pp. 8887–8896, Nov. 2017, doi: 10.1109/TIE.2017.2652402.

[5] H. Bayat and A. Yazdani, "A power mismatch elimination strategy for an MMC-based photovoltaic system," *IEEE Trans. Energy Convers.*, vol. 33, no. 3, pp. 1519–1528, Sep. 2018, doi: 10.1109/TEC.2018.2819982.

[6] Z. Zhao, D. Tan, and K. Li, "Transient behaviors of multiscale megawatt power electronics systems—Part I: Characteristics and analysis," *IEEE J. Emerg. Sel. Top. Power Electron.*, vol. 7, no. 1, pp. 7–17, Mar. 2019, doi: 10.1109/JESTPE.2019.2894424.

[7] D. Wang *et al.*, "A 10-kV/400-V 500-kVA electronic power transformer," *IEEE Trans. Ind. Electron.*, vol. 63, no. 11, pp. 6653–6663, Nov. 2016, doi: 10.1109/TIE.2016.2586440.

[8] K. Wang, R. Zhu, C. Wei, F. Liu, X. Wu, and M. Liserre, "Cascaded multilevel converter topology for large-scale photovoltaic system with balanced operation," *IEEE Trans. Ind. Electron.*, vol. 66, no. 10, pp. 7694–7705, Oct. 2019, doi: 10.1109/TIE.2018.2885739.

[9] M. R. Islam, A. M. Mahfuz-Ur-Rahman, K. M. Muttaqi, and D. Sutanto, "State-of-the-Art of the medium-voltage power converter technologies for grid integration of solar photovoltaic power plants," *IEEE Trans. Energy Convers.*, vol. 34, no. 1, pp. 372–384, Mar. 2019, doi: 10.1109/TEC.2018.2878885.

[10] S. Kouro, C. Fuentes, M. Perez, and J. Rodriguez, "Single DC-link cascaded H-bridge multilevel multistring photovoltaic energy conversion system with inherent balanced operation," in *Proc. IECON 38th Annu. Conf. IEEE Ind. Electron. Soc.*, Montreal, QC, Canada, Oct. 2012, pp. 4998–5005. doi: 10.1109/IECON.2012.6388983.

[11] B. Xiao, L. Hang, J. Mei, C. Riley, L. M. Tolbert, and B. Ozpineci, "Modular cascaded H-bridge multilevel PV inverter with distributed MPPT for grid-connected applications," *IEEE Trans. Ind. Applicat.*, vol. 51, no. 2, pp. 1722–1731, Mar. 2015, doi: 10.1109/TIA.2014.2354396.

[12] Y. Zhuang, F. Liu, Y. Huang, X. Zhang, and X. Zha, "A voltage-balancer-based cascaded DC–DC converter with a novel power feedforward control for the medium-voltage DC grid interface of photovoltaic systems," *IEEE Access*, vol. 7, pp. 178094–178107, 2019, doi: 10.1109/ACCESS.2019.2959040.

[13] H. Jafarian, N. Kim, and B. Parkhideh, "A distributed active and reactive power control strategy for balancing grid-tied cascaded H-bridge PV inverter system," in *Proc. IEEE Energy Convers. Congr. Expo.*, Cincinnati, OH, USA, Oct. 2017, pp. 1667–1672. doi: 10.1109/ECCE.2017.8095993.

[14] L. Liu, H. Li, and Y. Xue, "A coordinated active and reactive power control strategy for grid-connected cascaded photovoltaic (PV) system in high voltage high power applications," in *Proc. Twenty-8th Annu. IEEE Appl. Power Electron. Conf. Expo.*, Long Beach, CA, USA, Mar. 2013, pp. 1301–1308. doi: 10.1109/APEC.2013.6520467.

[15] L. Liu, H. Li, Y. Xue, and W. Liu, "Reactive power compensation and optimization strategy for grid-interactive cascaded photovoltaic systems," *IEEE Trans. Power Electron.*, vol. 30, no. 1, pp. 188–202, Jan. 2015, doi: 10.1109/TPEL.2014.2333004.

[16] F. V. Amaral, T. M. Parreiras, G. C. Lobato, A. A. P. Machado, I. A. Pires, and B. de Jesus Cardoso Filho, "Operation of a grid-tied cascaded multilevel converter based on a forward solid-state transformer under unbalanced PV power generation," *IEEE Trans. Ind. Applicat.*, vol. 54, no. 5, pp. 5493–5503, Sep. 2018, doi: 10.1109/TIA.2018.2827002.

[17] J. Lamb, B. Mirafzal, and F. Blaabjerg, "PWM common mode reference generation for maximizing the linear modulation region of CHB converters in islanded microgrids," *IEEE Trans. Ind. Electron.*, vol. 65, no. 7, pp. 5250–5259, Jul. 2018, doi: 10.1109/TIE.2017.2777401.

[18] J. Lamb and B. Mirafzal, "Grid-interactive cascaded H-bridge multilevel converter PQ plane operating region analysis," *IEEE Trans. Ind. Appl.*, vol. 53, no. 6, pp. 5744–5752, Nov./Dec. 2017.

[19] Y. Ko, M. Andresen, G. Buticchi, and M. Liserre, "Power routing for cascaded H-bridge converters," *IEEE Trans. Power Electron.*, vol. 32, no. 12, pp. 9435–9446, Dec. 2017, doi: 10.1109/TPEL.2017.2658182.

[20] T. Zhao *et al.*, "An optimized third harmonic compensation strategy for single-phase cascaded H-bridge photovoltaic inverter," *IEEE Trans. Ind. Electron.*, vol. 65, no. 11, pp. 8635–8645, Nov. 2018, doi: 10.1109/TIE.2018.2813960.

[21] A. K. Morya and A. Shukla, "Space vector modulated cascaded H-bridge multilevel converter for grid integration of large scale photovoltaic power plants," in *Proc. 4th Int. Conf. Power Eng., Energy Elect. Drives*, Istanbul, Turkey, May 2013, pp. 181–186. doi: 10.1109/PowerEng.2013.6635603.

[22] C. Wang, K. Zhang, J. Xiong, Y. Xue, and W. Liu, "An efficient modulation strategy for cascaded photovoltaic systems suffering from module mismatch," *IEEE J. Emerg. Sel. Top. Power Electron.*, vol. 6, no. 2, pp. 941–954, Jun. 2018, doi: 10.1109/JESTPE.2017.2756338.

[23] R. P. Aguilera *et al.*, "Predictive control of cascaded H-bridge converters under unbalanced power generation," *IEEE Trans. Ind. Electron.*, vol. 64, no. 1, pp. 4–13, Jan. 2017, doi: 10.1109/TIE.2016.2605618.

MIN CHEN (Senior Member, IEEE) was born in China, in 1976. He received the B.S. and Ph.D. degrees in power electronics from the Department of Electrical Engineering, Zhejiang University, Hangzhou, China, in 1998 and 2004, respectively. He is currently an Associate Professor with Zhejiang University. His research interests include power device packaging, high-frequency high-power conversion, and renewable energy power conversion system. He is an Associate Editor for the IEEE OPEN JOURNAL OF POWER ELECTRONICS.

YUFEI JIE was born in China, in 1998. He received the B.S. degree from the School of Electrical Engineering, Southeast University, Nanjing, China, in 2020. He is currently working toward the M.S. degree in electrical engineering with Zhejiang University, Hangzhou, China. His research interests include high-efficiency dc-dc converters, grid-connected inverters, and renewable energy applications.

CHU WANG received the B.S. degree from the University of Electronic Science and Technology of China, Chengdu, China, in 2018, and the M.S. degree from Zhejiang University, Hangzhou, China, in 2021. He is currently an Analyst of Value Rising Asset Management Co., Ltd. His main research interests include semiconductor industry and power market.

GONGHENG LI was born in 1999, Shandong province, China. He received the B.S. degree in electrical engineering in 2021 from Zhejiang University, Hangzhou, China, where he is currently working toward the M.S. degree in electrical engineering. His current research interests include power imbalance and inverters in photovoltaic systems.

LIN QIU (Member, IEEE) received the B.S. and Ph. D. degree in electrical engineering from the Department of Electrical Engineering, Tsinghua University, Beijing, China, in 2011 and 2017, respectively. He is currently a Research Fellow of electrical engineering with Zhejiang University, Hangzhou, China. His current research interests include converter topologies, smart transportation, and space power systems.

WENXING ZHONG (Senior Member, IEEE) received the B.S. degree in electrical engineering from Tsinghua University, Beijing, China, in 2007, and the Ph.D. degree from the City University of Hong Kong, Hong Kong, in 2012. He is currently a Professor with the Department of Electrical Engineering, Zhejiang University, Hangzhou, China. From March 2016 to May 2017, he was a Research Assistant Professor with the Department of Electrical and Electronic Engineering, University of Hong Kong, Hong Kong. His research interests include wireless power transfer and power electronics. He was the recipient of the two Transactions First Prize Paper Awards from IEEE Power Electronics Society.